Published in final edited form as:

Magn Reson Imaging. 2020 January ; 65: 27–36. doi:10.1016/j.mri.2019.09.007.

Magnetic resonance imaging (MRI) studies of Knee joint under mechanical loading: review

Saeed Jerban[a], **Eric Y. Chang**[b,a], **Jiang Du**[a]

[a]Department of Radiology, University of California, San Diego, CA, USA

[b]Radiology Service, VA San Diego Healthcare System, San Diego, CA, USA

Abstract

Osteoarthritis (OA) is a very common disease that affects the human knee joint, particularly the articular cartilage and meniscus components which are regularly under compressive mechanical loads. Early-stage OA diagnosis is essential as it allows for timely intervention. The primary non-invasive approaches currently available for OA diagnosis include magnetic resonance imaging (MRI), which provides excellent soft tissue contrast at high spatial resolution. MRI-based knee investigation is usually performed on joints at rest or in a non-weight-bearing condition that does not mimic the actual physiological condition of the joint. This discrepancy may lead to missed detections of early-stage OA or of minor lesions. The mechanical properties of degenerated musculoskeletal (MSK) tissues may vary markedly before any significant morphological or structural changes detectable by MRI. Recognizing distinct deformation characteristics of these tissues under known mechanical loads may reveal crucial joint lesions or mechanical malfunctions which result from early-stage OA. This review article summarizes the large number of MRI-based investigations on knee joints under mechanical loading which have been reported in the literature including the corresponding MRI measures, the MRI-compatible devices employed, and potential challenges due to the limitations of clinical MRI sequences.

Keywords

Knee; cartilage; meniscus; Osteoarthritis; MRI; loading

1. Introduction

The Knee joint consists of different tissues with various structural and mechanical properties. Articular cartilage and meniscus are two important components of the knee that are regularly under compressive mechanical loads. Collagen, the most abundant structural macromolecule in the extracellular matrix (ECM), makes up approximately 60–70% of the dry weight of cartilage and meniscus. Type II collagen represents majority of the collagen content in the cartilage and meniscal white-white zone, forming fibrils and fibers intertwined

Corresponding authors: Saeed Jerban. Department of Radiology, University of California, 9500 Gilman Dr., San Diego, CA 92093, USA, sjerban@ucsd.edu, Phone: +1 858 246 3158, Fax : +1 888 960 5922.

7.Conflict of interest statement

The authors have no conflicts of interest to declare.

with proteoglycan (PG) aggregates [1-5]. It should be noted that in red-red meniscal zone the type I collagen is predominant [5,6].

Osteoarthritis (OA) is one of the most prevalent diseases in the world, affecting a large global population and targeting the human knee joint in particular. OA patients may be unable to perform the usual activities of daily living, resulting in increased health costs for many nations [7]. The major public health issues associated with OA are likely to become even more challenging as society ages. Magnetic resonance imaging (MRI) is the most promising non-invasive technique for OA diagnosis, as it provides excellent soft tissue contrast at high spatial resolution and allows accurate morphological assessment [8-13]. However, conventional clinical MRI performs poorly in the detection and diagnosis of early-stage OA [14,15].

MRI-based investigation usually takes place on knee joints at rest or in a non-weight-bearing orientation–conditions which do not mimic the actual physiological condition of the joint. This may lead to missed detection of early-stage OA. Moreover, PG loss and structural changes in collagen fibrils in articular cartilage during early-stage OA can significantly alter the mechanical properties of the tissue [1,16,17]. Joint mechanical malfunction due to early-stage OA can be revealed by recognizing distinct deformation characteristics of MSK tissues under known mechanical loads. To investigate such hypotheses, many MRI-based studies on knee joints have been performed under mechanical loading for the purpose of detecting disease-specific changes in the knee. This article is devoted to summarizing the MRI-based studies performed on knees under mechanical loading, associated MRI measures, MRI-compatible devices employed in these studies, and potential challenges due to the limitations of conventional MRI sequences.

3. Subject positioning, vertical or supine

The reported MRI-based investigations of knee joints under loading have been performed primarily using the following two approaches. In the first approach, patients are placed in a vertical standing position and are scanned using an open-bore interventional MRI scanner [18-21]. In the second approach, patients are placed in a horizontal supine position and are scanned using a common clinical MRI (closed-bore) scanner, where the mechanical load is applied using an MRI-compatible loading device [22-50]. Open-bore interventional MRIs provide low magnetic field strengths and are less accessible in clinics [18]; therefore, the second approach employing clinical MRI-compatible devices to apply loading in knee studies has received more investigational attention. The latter approach is the focus of our review. It should be noted that due to the importance of knee function under loading, other imaging techniques have also been used to study knee joint variations under mechanical loading [51-53].

3. MRI measures and biomarkers

There are three main MRI measures which have been investigated through knee loading studies in the literature. Summary of MRI-based loading studies performed on whole knee joints are presented in Table 1. The output MRI measures in knee loading studies reported in

the literature can be categorized as 1) tissue deformation and morphological changes directly from magnitude images, 2) tissue deformation from MRI phase information, and 3) quantitative MRI.

3.1 Deformations from magnitude images

In the first group of studies, morphological changes in articular cartilage and meniscus, such as their thickness. In this approach images are segmented, surface meshes are created using a marching cubes algorithm, from which minimum distances between the reconstructed surfaces are evaluated at each mesh point to define the cartilage thickness. MRI images from gradient or spin echo sequences with relatively high image resolution (~0.3 mm in plane pixel size) were used in this group of studies. Herberhold et al. studied the effect of applied load on the deformation of human patellar/femoral cartilage of cadaveric knee joint using a fat-suppressed 3D gradient echo sequence (fast low angle shot, FLASH sequence) at a resolution of 0.3×0.3×2 mm^3 [28,29]. They reported continuous cartilage thickness reduction for 200 minutes under loading. Song et al. studied sheep knee cartilage deformation for joints undergoing partial meniscus removal using T1-weighted gradient echo imaging [30]. Following meniscectomy, they reported a significant decrease in the contact area and a significant increase in maximum cartilage deformation. Cotofana et al. employed an *in vivo* loading device to study the cartilage thickness variation under loading compared between a control group and an OA group [44]. They used spoiled gradient echo (SPGR) sequence with approx. 0.4×0.8×1.5 mm^3 voxel size. They reported a statistically significant reduction in cartilage thickness for medial tibia and femoral contact points. Shin et al. [42] investigated tibiofemoral contact area changes under loading in vivo using SPGR (approximately 0.3×0.3×1.5 mm^3 voxel size) and T2-weighted FSE sequences (approximately 0.3×0.4×2 mm^3 voxel size) in medical and lateral compartments of the joint in 10 healthy and 11 OA human knee joints. Tibiofemoral contact areas in both compartments significantly increased under loading, with greater increases in the medial joint. For both unloaded and loaded conditions, medial joint showed larger contact areas in OA joints. Subburaj et al. used the same device to measure in vivo tibiofemoral cartilage deformation in 10 healthy and 20 OA subjects using SPGR and FSE protocols with 0.3×0.3×2 mm^3 voxel size [46]. Higher cartilage thickness changes were found in medial compartment of the joint compared with lateral compartment of the joint of both normal and OA subjects. The average cartilage deformation was higher in OA joints versus normal joints (T1ρ and T2 were also investigated and will be discussed later in this review).

Wang et al. [26] employed an *in vivo* loading device and studied the cartilage thickness variation using 3D-SPGR sequence with an approximately 0.3×0.3×1.5 mm^3 voxel size. In addition to measuring thickness, they developed a technique to calculate the strain map of cartilage by comparing the obtained cartilage thickness maps before and during mechanical loading. They found significant strain increases in medial and lateral compartments of the femoral cartilages as well as in lateral compartment of the tibial cartilages by loading. Later, Maher et al. employed this technique to study the effect of applied load on the knee joints of young active patients undergoing meniscus allograft transplantation [27]. They also compared their MRI-based technique with direct contact force measurements using temporarily placed thin sensors in the joint during the surgery. The MR-based cartilage

deformation and contact stress maps within each subject map showed similar patterns. The majority of patients exhibited decreased peak contact stress and increased contact area after grafting.

Most of the knee loading studies in open-bore interventional MRIs were focused on distance transform and pixels' number estimations to investigate morphological variations of cartilage with lower spatial resolution in comparison with clinical MRIs [18-21].

Following the first group of studies focused on knee morphological changes under loading, Stehling et al. [43] investigated the effect of applied load on different knee structures in 10 healthy and 11 OA human knee joints in vivo. They reported significantly greater increases in meniscus extrusion under loading for degenerated knees compared with normal knees. Moreover, in knees with higher OA scores, loading resulted in larger morphological changes in meniscus and cartilage. Patel et al. [50] also used a similar loading device to measure the meniscus extrusion length on 3D FSE CUBE images before and during loading in 56 normal and 78 OA individuals. Differences in medial meniscal extrusion between loading and unloading were significant in the entire cohort. However, for knees in the healthy group, the extrusion variation was less compared with the moderate OA group.

3.2 Deformations from MRI phase data

In the second group of studies, cartilage deformation was estimated using sub-voxel displacement encoding techniques based on MRI phase data in order to calculate the cartilage strains. Neu and Walton developed a displacement encoding technique based on phase data obtained from FSE images (DENSE-FSE) to measure the deformation and strain of a cartilage specimen under loading [33]. Chan et al. used an *ex vivo* loading device to study cartilage strain variation in tibiofemoral cartilage of porcine knee joints under mechanical loading using the DENSE-FSE technique [36,37]. Later, Butz et al. used the same technique for MRI data acquisition and further developed a finite element model for measuring the mechanical stress from the estimated strains in the porcine tibiofemoral cartilage and the known applied loads [38]. Chan et al. employed an *in vivo* loading setup with a similar structure to apply loads on the knee joints of 9 normal individuals and subsequently to quantify the mechanical behavior of tibiofemoral articular cartilage [31]. They reported correlations between body mass index and maximum principle and shear strain measures in tibial cartilage. Recently, Zevenbergen et al. examined the sensitivity of this technique to changes in bovine tibiofemoral cartilage induced by synthetic defects [39]. They reported elevated strains at the defect regions of the cartilage, where the opposing cartilage showed minimal increase in strain patterns.

3.3 Quantitative MRI

In the third group of studies, quantitative MRI properties such as delayed gadolinium-enhanced T_1, T2, and $T_{1\rho}$ in knee tissues were measured under mechanical loading. Quantitative MRI properties provide microstructural and compositional information regarding PG, collagen, and water pools in the knee tissues; hence, they are more appealing for MRI-based knee loading studies. Specifically, $T_{1\rho}$ has been shown to be sensitive to PG depletion [54,55], while T_2 is sensitive to collagen degradation and water pool changes

[56,57]. Rubenstein et al. examined T2 variation in bovine cartilage specimens under static compression and observed a gradually decreasing MRI T2 signal [58]. They also found a reversal change in MRI signal after releasing the mechanical load. Kaufman et al. observed a gradual reduction in T1 and T2 values of articular bovine cartilage specimens at a continuous constant pressure [59]. The decrease in MRI signals over time was explained by increased deformation and accordingly increased water loss under constant mechanical loading [58,59]. Nebelung et al. studied T2 variation under mechanical loading in human cartilage specimens [25,60,61]. They observed T2 reduction in the studied human cartilage specimen. Other studies investigating T2, T1, and T1-Gd MRI variations in cartilage specimens under mechanical loading observed different patterns of variations depending on the investigated zone of the cartilage, likely a result of the magic angle phenomenon in MRI [62-67].

Following the third group of studies focused on quantitative MRI under loading, Shiomi et al. studied T2 variations in the tibiofemoral cartilage of 10 intact porcine joints ex vivo under loading [24]. They found the greatest decrease of T2 to be in the intermediate zone of the cartilage. The T2 reduction correlated with contact pressure measured with sensitive films placed in the knee joints. Later, Shiomi et al. examined tibiofemoral cartilage T2 variations under loading in 10 porcine joints ex vivo before and after meniscectomy [68]. They reported shifted regions of large T2 decreases under loading from anterior/central sites to the posterior sites in medial joint. Nishii et al. studied the in vivo T2 variation in human tibiofemoral cartilage of 22 normal volunteers under compression [23]. T2 decreased under loading over the tibial cartilage, but only in the contact region with the femoral cartilage. Mayerhoefer et al. studied the in vivo loading effect on the delayed gadolinium-enhanced MRI of tibiofemoral cartilage (dGEMRIC) relaxation time (T1-Gd) in normal knee joints [22]. They observed a significant decrease in average T1-Gd for joints under loading. Souza et al. studied the effects of acute loading on T1ρ and T2 relaxation times in human tibiofemoral cartilage of 20 OA and 10 control knees [34]. They found significant reductions of T2 and T1ρ only at the medial joint under mechanical loading. Subburaj et al. compared T1ρ and T2 variations under loading between 20 OA and 10 control individuals at different tibiofemoral cartilage layers [46]. They found greater T1ρ and T2 reductions at the superficial tibiofemoral cartilage layer, whereas the deep regions showed an increase in T1ρ and T2. Later, Souza et al. compared the T1ρ and T2 variations of tibiofemoral cartilage under loading between 99 normal and 44 OA human subjects [47]. Significant T1ρ reduction was found in the medial and lateral compartments of the tibial cartilage for both groups. Specifically, they reported significant decreases for T1ρ and T2 measures at the superficial layer of the cartilage, yet significant increases were found at the deep layer of the cartilage. T1ρ and T2 reductions were greater for subjects with OA (13-19%) when compared to healthy controls (3-13%). Szomolanyi et al. [41] examined the in vivo T2 variations in tibiofemoral cartilage of 10 healthy volunteers under loading at 7 T. They reported T2 reduction for regions under loading and T2 increase for regions adjacent to loadbearing cartilage.

Subburaj et al. investigated T2 and $T_{1\rho}$ differences under loading in the meniscus of 20 OA patient and 10 controls [48]. They reported T2 and $T_{1\rho}$ increases in meniscus under loading. Significantly higher variations under loading were reported for controls compared with OA

subjects. Calixto et al. investigated the T2 and $T_{1\rho}$ differences under loading in the menisci of 85 healthy and 39 OA human subjects at three different zones [49]. A significant increase with loading was seen in the T2 of the control group, while T2 increase was less frequently observed in subjects with OA. Hornakova et al. [40] studied the T2* variation in meniscus of four healthy individuals and reported a constant significant increase of T2* after compression in the anterior horn of the medial meniscus up to 40 minutes after loading.

All major knee tissues are viscoelastic materials with time-dependent behavior when subjected to a constant load (i.e., creep) or deformation (e.g., stress relaxation) [2,69]. Elastic and viscoelastic properties of cartilage have been discussed in various *ex vivo* experiments [1,16,17,58,59,70-73]. The lasting variation of knee joints after mechanical load application and unloading have been indirectly investigated in several studies by analyzing the prospective impact of physical activity on MRI measures [45,74-81].

4. MRI-compatible loading devices

MRI-compatible loading devices employed in the literature can be classified mainly as passive or active loading devices. The primary advantages of the passive loading devices are simplicity and availability; however, adjustment of the applied force in these devices is both limited and challenging during the MRI scanning. Passive loading devices used in the literature can be classified in the three following groups. First, a large number of knee loading studies used cable/pulley setups, where the gravity force applied on suspended weights was transferredd to the individuals' feet. Nishii et al. used a cable/pulley setup combined with a backboard and a sliding foot plate on low friction rollers to position the subject, then employed water-level weights for loading [23]. Souza et al. employed a similar loading setup using solid non-ferromagnetic weights [34]. Similar *in vivo* loading devices were used in several other studies [42-50,82]. Second, a smaller group of studies used ratcheting mechanisms driving an orthotic boot to apply mechanical loads to the subjects' feet where an MRI-compatible load cell was attached to estimate the applied load [26,27,83]. Third, another group of studies (mostly *ex vivo* investigations) employed screw-driven non-ferromagnetic elastic elements to apply the mechanical loads. Shiomi et al. employed a sliding plate bounded by a viscoelastic foam material (poly-olefin elastomer) to load porcine knee specimens. The foam was compressed by a manually derived screw on one end [24]. In other research studies, miniature MRI-compatible loading devices were utilized to apply loads on human or animal cartilage specimens using screw-driven indenters fabricated from plastic parts [25,60-66]. Recently, Hornakova et al. [40] employed tightened rubber bands attaching to the subject's waist and feet for loading knees *in vivo*, while the applied forces could be measured using dynamometric insoles.

In the active loading devices, an electromechanical, pneumatic, or hydraulic actuator is used to apply the force. The active loading devices allow more precise control of the applied forces during MRI scans, providing the option of time-dependent force application. Miniature pneumatic or electro-pneumatic systems have been reported in several studies for the purpose of load application on human or animal cartilage specimens during MRI scanning [33,58,59]. Herberhold et al. developed an MRI-compatible electro-pneumatic actuator to apply mechanical loads on bent human cadaver knee joints [28,29]. Song et al.

also used a pneumatic actuator to load the sheep knee joint [30]. Mayerhoefer et al. used a custom-made pneumatic actuator to load human knee joints scanned *in vivo* on a clinical MRI using a flexible coil [22]. The upper end of the actuator was attached to the femur while the lower end was attached to the footplate. Szomolanyi et al. [41] also used a pneumatic actuator to load human knee joints scanned *in vivo* on a 7T MRI using a knee coil. Martin et al. used an electro-pneumatic device to load cadaver knee joints on clinical MRI where both ends of the joint were mounted in PMMA modeled clamps [35,84]. Chan et al. also used electro-pneumatic actuators to apply cyclic loading on porcine joints [36-38] and cartilage specimens [39] during MRI scans. Later, Chan et al. used electro-pneumatic actuators for *in vivo* load application on human knee joints [31]. The load was applied to the footplate where the individual's shoulder was fixed with strips to the MRI bed.

5. Challenges and future investigations

5.1 Short T2 tissues challenge clinical MRI in knee joint

Clinical MRI provides excellent soft tissue contrast at high spatial resolution and allows accurate assessment of longitudinal changes in cartilage morphology [8-13,85-87]. Unfortunately, clinical MRI sequences can only assess tissues with relatively long T2s, such as the superficial layers of articular cartilage. Many joint tissues, including the deep layers of articular cartilage, menisci, ligaments, tendons, and bone have short or ultrashort T2s and show little signal with clinical sequences [3,88-90]. It should be noted that T2 values between 0.1–1ms, 1–10ms, and above 10ms can be referred to as ultrashort, short, and long T2, respectively, in the literature[3]. Consequently, knee loading studies using clinical MRI are challenging because a large portion of cartilage and meniscus cannot be imaged properly.

Ultrashort echo time MRI (UTE-MRI) sequences, first introduced in 1989 [91], are among the most progressive techniques to image and quantify both short and long T_2 tissues in the knee joint [3,92]. UTE-MRI can image short T_2 MSK tissues with a high signal. With UTE-MRI, signal is acquired after radiofrequency (RF) excitation, as quickly as allowed by the RF hardware (tens of microseconds or shorter), before major decay in transverse magnetizations of the deep layers of articular cartilage, menisci, and other short T2 tissues. UTE-MRI has been investigated by many research groups for quantitative assessment of menisci and articular cartilage. Qian et al. studied multi-component fitting of UTE-MRI T2* in cartilage specimens [93]. Williams et al. used UTE-MRI T2* to assess the degeneration of human cartilage specimens [94]. UTE-MRI T2* values were found to be lower in severely degraded cartilage compared with healthy tissues. In a later study, they investigated the feasibility and repeatability of the UTE-MRI T2* modeling technique *in vivo* [95]. They found that UTE-MRI T2* can detect sub-clinical injuries in the meniscus [96]. Shao et al. used the bicomponent exponential fitting model for UTE-MRI T2* analysis in patellar cartilage specimens [97]. Goto et al. reported *in vivo* UTE-MRI T2* analysis in knee cartilage based on spiral MRI data acquisition [98]. Bae et al. [99] and Ma et al. [100] employed the UTE-MRI to visualize and quantify specifically the deep layer of articular cartilage. There is still a gap in the literature regarding the use of UTE-MRI techniques in knee loading studies.

5.2 Orientation-sensitivity in MRI quantifications (magic angle effect)

Extensive MRI-based research in knee loading studies has focused on T1ρ, T2, and T2* biomarkers. The principal confounding factor in $T_{1\rho}$, T2, and T2* measurements is the orientation sensitivity of these techniques, known as the "magic angle effect" [101-110]. This may result in a several fold increase in $T_{1\rho}$, T2, and T2*, as well as significant zonal contrast alterations depending on the fiber type and the orientation angle relative to B_0 (MRI bore axis) [62-66,110-116]. Orientation-based changes may exceed the changes caused by the loading, and may complicate interpretation of altered $T_{1\rho}$s, T2s, and T2*s. Although UTE-MRI sequences have made significant progress in imaging short T_2 tissues in the knee joint, regular UTE biomarkers, such as $UTET_{1\rho}$, T2*, and bi-component T2* analyses, are also sensitive to the magic angle effect [110,117]. However, the combinations of UTE with adiabatic $T_{1\rho}$ (UTE-Adiab-$T_{1\rho}$) and MT (UTE-MT) have recently been shown to be insensitive to orientation, suggesting that UTE-Adiab-$T_{1\rho}$ and UTE-MT have the potential to provide more robust evaluation of MSK tissue composition [118-120]. Nevertheless, performance of orientation-insensitive MRI technique such as UTE-Adiab-$T_{1\rho}$ and UTE-MT variations in knee loading studies needs to be investigated further in the literature.

6. Conclusions

Knee MRI-based studies performed under mechanical loading were reviewed. Knee loading studies were classified based on the investigated MRI measures, MRI techniques, as well as the MRI-compatible devices employed. Limitations of the studied quantitative MRI sequences such as orientation sensitivity and the incapability of imaging short T2 tissues in the knee joint were discussed. The orientation-insensitive MRI techniques developed for short T2 tissues, such as UTE-Adiab-$T_{1\rho}$ and UTE-MT, were suggested for future knee loading investigations.

Acknowledgements

The authors acknowledge grant support from NIH (1R01AR062581-01A1, 1R21AR073496, R01AR068987) and VA Clinical Science and Rehabilitation R&D (I01CX001388 and I01RX002604).

9. References

[1]. Mansour JM. Biomechanics of Cartilage. Kinesiol Mech Pathomechanics Hum Mov 2009:66–79. doi:10.1002/art.23548.

[2]. Sophia Fox a. J, Bedi a., Rodeo S a. The Basic Science of Articular Cartilage: Structure, Composition, and Function. Sport Heal A Multidiscip Approach 2009;1:461–8. doi: 10.1177/1941738109350438.

[3]. Chang EY, Du J, Chung CB. UTE imaging in the musculoskeletal system. J Magn Reson Imaging 2015;41:870–83. doi:10.1002/jmri.24713. [PubMed: 25045018]

[4]. López-Franco M, Gómez-Barrena E. Cellular and molecular meniscal changes in the degenerative knee: a review. J Exp Orthop 2018;5. doi:10.1186/s40634-018-0126-8.

[5]. Chevrier A, Nelea M, Hurtig MB, Hoemann CD, Buschmann MD. Meniscus structure in human, sheep, and rabbit for animal models of meniscus repair. J Orthop Res 2009;27:1197–203. doi: 10.1002/jor.20869. [PubMed: 19242978]

[6]. Makris EA, Hadidi P, Athanasiou KA. The knee meniscus: Structure-function, pathophysiology, current repair techniques, and prospects for regeneration. Biomaterials 2011;32:7411–31. doi: 10.1016/j.biomaterials.2011.06.037. [PubMed: 21764438]

[7]. Yelin E, Weinstein S, King T. The burden of musculoskeletal diseases in the United States. Semin Arthritis Rheum 2016;46:259–60. doi:10.1016/j.semarthrit.2016.07.013. [PubMed: 27519477]

[8]. Guermazi A, Roemer FW, Burstein D, Hayashi D. Why radiography should no longer be considered a surrogate outcome measure for longitudinal assessment of cartilage in knee osteoarthritis. Arthritis Res Ther 2011;13:247. doi:10.1186/ar3488. [PubMed: 22136179]

[9]. Recht MP, Goodwin DW, Winalski CS, White LM. MRI of Articular Cartilage: Revisiting Current Status and Future Directions. Am J Roentgenol 2005;185:899–914. doi:10.2214/ajr.05.0099. [PubMed: 16177408]

[10]. König H, Sauter R, Deimling M, Vogt M. Cartilage disorders: comparison of spin-echo, CHESS, and FLASH sequence MR images. Radiology 1987;164:753–8. doi:10.1148/radiology.164.3.3615875. [PubMed: 3615875]

[11]. Recht MP, Piraino DW, Paletta GA, Schils JP, Belhobek GH. Accuracy of fat-suppressed three-dimensional spoiled gradient-echo FLASH MR imaging in the detection of patellofemoral articular cartilage abnormalities. Radiology 1996;198:209–12. doi:10.1148/radiology.198.1.8539380. [PubMed: 8539380]

[12]. Disler DG, McCauley TR, Wirth CR, Fuchs MD. Detection of knee hyaline cartilage defects using fat-suppressed three-dimensional spoiled gradient-echo MR imaging: comparison with standard MR imaging and correlation with arthroscopy. Am J Roentgenol 1995;165:377–82. doi:10.2214/ajr.165.2.7618561. [PubMed: 7618561]

[13]. Bredella MA, Tirman PF, Peterfy CG, Zarlingo M, Feller JF, Bost FW, et al. Accuracy of T2-weighted fast spin-echo MR imaging with fat saturation in detecting cartilage defects in the knee: comparison with arthroscopy in 130 patients. Am J Roentgenol 1999;172:1073–80. doi:10.2214/ajr.172.4.10587150. [PubMed: 10587150]

[14]. Burstein D, BASHIR A, GRAY ML. MRI Techniques in Early Stages of Cartilage Disease. Invest Radiol 2000;35:622–38. doi:10.1097/00004424-200010000-00008. [PubMed: 11041156]

[15]. Eckstein F, Burstein D, Link TM. Quantitative MRI of cartilage and bone: degenerative changes in osteoarthritis. NMR Biomed 2006;19:822–54. doi:10.1002/nbm.1063. [PubMed: 17075958]

[16]. Juras V, Bittsansky M, Majdisova Z, Szomolanyi P, Sulzbacher I, Gäbler S, et al. In vitro determination of biomechanical properties of human articular cartilage in osteoarthritis using multi-parametric MRI. J Magn Reson 2009;197:40–7. doi:10.1016/j.jmr.2008.11.019. [PubMed: 19114313]

[17]. Desrochers J, Amrein MW, Matyas JR. Viscoelasticity of the articular cartilage surface in early osteoarthritis. Osteoarthr Cartil 2012;20:413–21. doi:10.1016/j.joca.2012.01.011. [PubMed: 22313971]

[18]. Shapiro LM, Gold GE. MRI of weight bearing and movement. Osteoarthr Cartil 2012;20:69–78. doi:10.1016/j.joca.2011.11.003. [PubMed: 22138286]

[19]. Powers CM, Ward SR, Fredericson M, Shellock FG. Knee Extension in Persons With Lateral Subluxation of the Patella: A Preliminary Study. J Orthop Sport Phys Ther 2003;33:677–87.

[20]. Gold GE, Besier TF, Draper CE, Asakawa DS, Delp SL, Beaupre GS. Weight-bearing MRI of patellofemoral joint cartilage contact area. J Magn Reson Imaging 2004;20:526–30. doi:10.1002/jmri.20146. [PubMed: 15332263]

[21]. Draper CE, Besier TF, Fredericson M, Santos JM, Beaupre GS, Delp SL, et al. Differences in patellofemoral kinematics between weight-bearing and non-weight-bearing conditions in patients with patellofemoral pain. J Orthop Res 2011;29:312–7. doi:10.1002/jor.21253. [PubMed: 20949442]

[22]. Mayerhoefer ME, Welsch GH, Mamisch TC, Kainberger F, Weber M, Nemec S, et al. The in vivo effects of unloading and compression on T1-Gd (dGEMRIC) relaxation times in healthy articular knee cartilage at 3.0 Tesla. Eur Radiol 2010;20:443–9. doi:10.1007/s00330-009-1559-3. [PubMed: 19727756]

[23]. Nishii T, Kuroda K, Matsuoka Y, Sahara T, Yoshikawa H. Change in knee cartilage T2 in response to mechanical loading. J Magn Reson Imaging 2008;28:175–80. doi:10.1002/jmri.21418. [PubMed: 18581338]

[24]. Shiomi T, Nishii T, Tanaka H, Yamazaki Y, Murase K, Myoui A, et al. Loading and knee alignment have significant influence on cartilage MRI T2 in porcine knee joints. Osteoarthr Cartil 2010;18:902–8. doi:10.1016/j.joca.2010.05.002. [PubMed: 20472084]

[25]. Nebelung S, Post M, Raith S, Fischer H, Knobe M, Braun B, et al. Functional in situ assessment of human articular cartilage using MRI: a whole-knee joint loading device. Biomech Model Mechanobiol 2017;16:1971–86. doi:10.1007/s10237-017-0932-4. [PubMed: 28685238]

[26]. Wang H, Koff MF, Potter HG, Warren RF, Rodeo SA, Maher SA. An MRI-compatible loading device to assess knee joint cartilage deformation: Effect of preloading and inter-test repeatability. J Biomech 2015;48:2934–40. doi:10.1016/j.jbiomech.2015.08.006. [PubMed: 26303166]

[27]. Maher SA, Wang H, Koff MF, Belkin N, Potter HG, Rodeo SA. Clinical platform for understanding the relationship between joint contact mechanics and articular cartilage changes after meniscal surgery. J Orthop Res 2017;35:600–11. doi:10.1002/jor.23365. [PubMed: 27410773]

[28]. Herberhold C, Faber S, Stammberger T, Steinlechner M, Putz R, Englmeier KH, et al. In situ measurement of articular cartilage deformation in intact femoropatellar joints under static loading. J Biomech 1999;32:1287–95. doi:10.1016/S0021-9290(99)00130-X. [PubMed: 10569707]

[29]. Herberhold C, Stammberger T, Faber S, Putz R, Englmeier KH, Reiser M, et al. An MR-based technique for quantifying the deformation of articular cartilage during mechanical loading in an intact cadaver joint. Magn Reson Med 1998;39:843–50. doi:10.1002/mrm.1910390522. [PubMed: 9581616]

[30]. Song Y, Greve JM, Carter DR, Koo S, Giori NJ. Articular cartilage MR imaging and thickness mapping of a loaded knee joint before and after meniscectomy. Osteoarthr Cartil 2006;14:728–37. doi:10.1016/j.joca.2006.01.011. [PubMed: 16533610]

[31]. Chan DD, Cai L, Butz KD, Trippel SB, Nauman EA, Neu CP. In vivo articular cartilage deformation: noninvasive quantification of intratissue strain during joint contact in the human knee. Sci Rep 2016;6:19220. doi:10.1038/srep19220. [PubMed: 26752228]

[32]. Neu CP. Functional imaging in OA: Role of imaging in the evaluation of tissue biomechanics. Osteoarthr Cartil 2014;22:1349–59. doi:10.1016/j.joca.2014.05.016. [PubMed: 25278049]

[33]. Neu CP, Walton JH. Displacement encoding for the measurement of cartilage deformation. Magn Reson Med 2008;59:149–55. doi:10.1002/mrm.21464. [PubMed: 18050342]

[34]. Souza RB, Stehling C, Wyman BT, Hellio Le Graverand MP, Li X, Link TM, et al. The effects of acute loading on T1rho and T2 relaxation times of tibiofemoral articular cartilage. Osteoarthr Cartil 2010;18:1557–63. doi:10.1016/j.joca.2010.10.001. [PubMed: 20950693]

[35]. Martin KJ, Neu CP, Hull ML. Quasi-steady-state displacement response of whole human cadaveric knees in a MRI scanner. J Biomech Eng 2009;131:081004. doi:10.1115/1.2978986. [PubMed: 19604016]

[36]. Chan DD, Neu CP, Hull ML. Articular cartilage Deformation determined in an intact tibiofemoral joint by displacement-encoded imaging. Magn Reson Med 2009;61:989–93. doi:10.1002/mrm.21927. [PubMed: 19189290]

[37]. Chan DD, Neu CP, Hull ML. In situ deformation of cartilage in cyclically loaded tibiofemoral joints by displacement-encoded MRI. Osteoarthr Cartil 2009;17:1461–8. doi:10.1016/j.joca.2009.04.021. [PubMed: 19447213]

[38]. Butz KD, Chan DD, Nauman EA, Neu CP. Stress distributions and material properties determined in articular cartilage from MRI-based finite strains. J Biomech 2011;44:2667–72. doi:10.1016/j.jbiomech.2011.08.005. [PubMed: 21920526]

[39]. Zevenbergen L, Gsell W, Chan DD, Vander Sloten J, Himmelreich U, Neu CP, et al. Functional assessment of strains around a full-thickness and critical sized articular cartilage defect under compressive loading using MRI. Osteoarthr Cartil 2018;26:1710–21. doi:10.1016/j.joca.2018.08.013. [PubMed: 30195045]

[40]. Hornakova L, Juras V, Kubovy P, Hadraba D, Gerych D, Stursa P, et al. In vivo assessment of time dependent changes of T2* in medial meniscus under loading at 3T: A preliminary study. J Appl Biomed 2018;16:138–44. doi:10.1016/j.jab.2017.12.001. [PubMed: 30022865]

[41]. Szomolanyi P, Rohrich S, Frollo I, Juras V, Schreiner M, Heule R, et al. Evaluation of compression properties of human knee cartilage-In-vivo study at 7T MRI. 2017 11th Int. Conf. Meas. Meas. 2017 - Proc., 2017, p. 185–8. doi:10.23919/MEASUREMENT.2017.7983567.

[42]. Shin CS, Souza RB, Kumar D, Link TM, Wyman BT, Majumdar S. In vivo tibiofemoral cartilage-to-cartilage contact area of females with medial osteoarthritis under acute loading using MRI. J Magn Reson Imaging 2011;34:1405–13. doi:10.1002/jmri.22796. [PubMed: 21953771]

[43]. Stehling C, Souza RB, Graverand MPH Le, Wyman BT, Li X, Majumdar S, et al. Loading of the knee during 3.0 T MRI is associated with significantly increased medial meniscus extrusion in mild and moderate osteoarthritis. Eur J Radiol 2012;81:1839–45. doi:10.1016/j.ejrad.2011.05.027. [PubMed: 21684704]

[44]. Cotofana S, Eckstein F, Wirth W, Souza RB, Li X, Wyman B, et al. In vivo measures of cartilage deformation: Patterns in healthy and osteoarthritic female knees using 3T MR imaging. Eur Radiol 2011;21:1127–35. doi:10.1007/s00330-011-2057-y. [PubMed: 21448616]

[45]. Souza RB, Baum T, Wu S, Feeley BT, Kadel N, Li X, et al. Effects of unloading on knee articular cartilage T1rho and T2 magnetic resonance imaging relaxation times: a case series. J Orthop Sports Phys Ther 2012;42:511–20. doi:10.2519/jospt.2012.3975. [PubMed: 22402583]

[46]. Subburaj K, Souza RB, Stehling C, Wyman BT, Le Graverand-Gastineau MP, Link TM, et al. Association of MR relaxation and cartilage deformation in knee osteoarthritis. J Orthop Res 2012;30:919–26. doi:10.1002/jor.22031. [PubMed: 22161783]

[47]. Souza RB, Kumar D, Calixto N, Singh J, Schooler J, Subburaj K, et al. Response of knee cartilage T1rho and T2 relaxation times to in vivo mechanical loading in individuals with and without knee osteoarthritis. Osteoarthritis Cartilage 2014;22:1367–76. doi:10.1016/j.joca.2014.04.017. [PubMed: 24792208]

[48]. Subburaj K, Souza RB, Wyman BT, Le Graverand-Gastineau MPH, Li X, Link TM, et al. Changes in MR relaxation times of the meniscus with acute loading: An in vivo pilot study in knee osteoarthritis. J Magn Reson Imaging 2015;41:536–43. doi:10.1002/jmri.24546. [PubMed: 24347310]

[49]. Calixto NE, Kumar D, Subburaj K, Singh J, Schooler J, Nardo L, et al. Zonal differences in meniscus MR relaxation times in response to in vivo static loading in knee osteoarthritis. J Orthop Res 2016;34:249–61. doi:10.1002/jor.23004. [PubMed: 26223430]

[50]. Patel R, Eltgroth M, Souza RB, Zhang CA, Majumdar S, Link TM, et al. Loaded versus unloaded magnetic resonance imaging (MRI) of the knee: Effect on meniscus extrusion in healthy volunteers and patients with osteoarthritis. Eur J Radiol Open 2016;3:100–7. doi:10.1016/j.ejro.2016.05.002. [PubMed: 27331081]

[51]. Kim TH, Sobti A, Lee SH, Lee JS, Oh KJ. The effects of weight-bearing conditions on patellofemoral indices in individuals without and with patellofemoral pain syndrome. Skeletal Radiol 2014;43:157–64. doi:10.1007/s00256-013-1756-7. [PubMed: 24221139]

[52]. Myers CA, Torry MR, Shelburne KB, Giphart JE, Laprade RF, Woo SLY, et al. In vivo tibiofemoral kinematics during 4 functional tasks of increasing demand using biplane fluoroscopy. Am J Sports Med 2012;40:170–8. doi:10.1177/0363546511423746. [PubMed: 21997729]

[53]. Wan L, De Asia RJ, Rubash HE, Li G. In vivo cartilage contact deformation of human ankle joints under full body weight. J Orthop Res 2008;26:1081–9. doi:10.1002/jor.20593. [PubMed: 18327792]

[54]. Duvvuri U, Reddy R, Patel SD, Kaufman JH, Kneeland JB, Leigh JS. T1ρ-relaxation in articular cartilage: Effects of enzymatic degradation. Magn Reson Med 1997;38:863–7. doi:10.1002/mrm.1910380602. [PubMed: 9402184]

[55]. Duvvuri U, Charagundla SR, Kudchodkar SB, Kaufman JH, Kneeland JB, Rizi R, et al. Human Knee: In Vivo T1ρ-weighted MR Imaging at 1.5 T—Preliminary Experience. Radiology 2001;220:822–6. doi:10.1148/radiol.2203001662. [PubMed: 11526288]

[56]. Mosher TJ, Dardzinski BJ. Cartilage MRI T2 Relaxation Time Mapping: Overview and Applications. Semin Musculoskelet Radiol 2004;08:355–68. doi:10.1055/s-2004-861764.

[57]. Liess C, Lüsse S, Karger N, Heller M, Glüer CG. Detection of changes in cartilage water content using MRI T2-mapping in vivo. Osteoarthr Cartil 2002;10:907–13. doi:10.1053/joca.2002.0847. [PubMed: 12464550]

[58]. Rubenstein JD, Kim JK, Henkelman RM. Effects of compression and recovery on bovine articular cartilage: appearance on MR images. Radiology 1996;201:843–50. doi:10.1148/radiology.201.3.8939241. [PubMed: 8939241]

[59]. Kaufman JH, Regatte RR, Bolinger L, Kneeland JB, Reddy R, Leigh JS. A novel approach to observing articular cartilage deformation in vitro via magnetic resonance imaging. J Magn Reson Imaging 1999;9:653–62. doi:10.1002/(SICI)1522-2586(199905)9:5<653::AID-JMRI6>3.0.CO;2-4. [PubMed: 10331760]

[60]. Nebelung S, Sondern B, Tingart M, Rath B, Pufe T, Raith S, et al. Functional MR Imaging Mapping of Human Articular Cartilage Response to Loading. Radiology 2017;000.

[61]. Nebelung S, Brill N, Muller F, Tingart M, Pufe T, Merhof D, et al. Towards Optical Coherence Tomography-based elastographic evaluation of human cartilage. J Mech Behav Biomed Mater 2016;56:106–19. doi:10.1016/j.jmbbm.2015.11.025. [PubMed: 26700573]

[62]. Alhadlaq HA, Xia Y. The structural adaptations in compressed articular cartilage by microscopic MRI (??MRI) T2 anisotropy. Osteoarthr Cartil 2004;12:887–94. doi:10.1016/j.joca.2004.07.006. [PubMed: 15501404]

[63]. Alhadlaq HA, Xia Y. Modifications of orientational dependence of microscopic magnetic resonance imaging T2 anisotropy in compressed articular cartilage. J Magn Reson Imaging 2005;22:665–73. doi:10.1002/jmri.20418. [PubMed: 16220547]

[64]. Lee J, Badar F, Kahn D, Matyas J, Qu X, Chen CT, et al. Topographical variations of the strain-dependent zonal properties of tibial articular cartilage by microscopic MRI. Connect Tissue Res 2014;55:205–16. doi:10.3109/03008207.2014.894997. [PubMed: 24559385]

[65]. Wang N, Badar F, Xia Y. MRI properties of a unique hypo-intense layer in degraded articular cartilage. Phys Med Biol 2015;8709:8709. doi:10.1088/0031-9155/60/22/8709.

[66]. Wang N, Kahn D, Badar F, Xia Y. Molecular origin of a loading-induced black layer in the deep region of articular cartilage at the magic angle. J Magn Reson Imaging 2015;41:1281–90. doi:10.1002/jmri.24658. [PubMed: 24833266]

[67]. Rautiainen J, Nissi MJ, Salo E-N, Tiitu V, Finnilä M a J, Aho O- M, et al. Multiparametric MRI assessment of human articular cartilage degeneration: Correlation with quantitative histology and mechanical properties. Magn Reson Med 2014;00:249–59. doi:10.1002/mrm.25401.

[68]. Shiomi T, Nishii T, Tamura S, Tanaka H, Murase K, Yoshikawa H, et al. Influence of medial meniscectomy on stress distribution of the femoral cartilage in porcine knees: A 3D reconstructed T2 mapping study. Osteoarthr Cartil 2012;20:1383–90. doi:10.1016/j.joca.2012.07.015. [PubMed: 22846714]

[69]. Lakes R Viscoelastic Materials. 2009. doi:10.1017/CBO9780511626722.

[70]. Akizuki S, Mow VC, Muller F, Pita JC, Howell DS. Tensile Properties of Human Knee Joint Cartilage . 11 . Correlations Between Weight Bearing and Tissue Pathology and the Kinetics of Swelling. J Orthop Res 1987;5:173–86. [PubMed: 3572588]

[71]. Sah RL, Doong JYH, Kim YJ, Grodzinsky AJ, Plaas AHK, Sandy JD. Biosynthetic response of cartilage explants to mechanical and physicochemical stimuli. TransOrthop ResSoc 1988;13:70.

[72]. Espino DM, Shepherd DET, Hukins DWL. Viscoelastic properties of bovine knee joint articular cartilage: dependency on thickness and loading frequency. BMC Musculoskelet Disord 2014;15:205. doi:10.1186/1471-2474-15-205. [PubMed: 24929249]

[73]. Deneweth JM, Newman KE, Sylvia SM, McLean SG, Arruda EM. Heterogeneity of tibial plateau cartilage in response to a physiological compressive strain rate. J Orthop Res 2013;31:370–5. doi:10.1002/jor.22226. [PubMed: 22952052]

[74]. Mosher TJ, Smith HE, Collins C, Liu Y, Hancy J, Dardzinski BJ, et al. Change in knee cartilage T2 at MR imaging after running: a feasibility study. Radiology 2005;234:245–9. doi:10.1148/radiol.2341040041. [PubMed: 15550376]

[75]. Mosher TJ, Liu Y, Torok CM. Functional cartilage MRI T2 mapping: evaluating the effect of age and training on knee cartilage response to running. Osteoarthr Cartil 2010;18:358–64. doi:10.1016/j.joca.2009.11.011. [PubMed: 19948266]

[76]. Liess C, Lusse S, Karger N, Heller M, Gluer CG. Detection of changes in cartilage water content using MRI T2-mapping in vivo. Osteoarthr Cartil 2002;10:907–13. doi:10.1053/joca.2002.0847. [PubMed: 12464550]

[77]. Eckstein F, Tieschky M, Faber SC, Haubner M, Kolem H, Englmeier KH, et al. Effect of physical exercise on cartilage volume and thickness in vivo: MR imaging study. Radiology 1998;207:243–8. doi:10.1148/radiology.207.1.9530322. [PubMed: 9530322]

[78]. Eckstein F, Lemberger B, Gratzke C, Hudelmaier M, Glaser C, Englmeier K-H, et al. In vivo cartilage deformation after different types of activity and its dependence on physical training status. Ann Rheum Dis 2005;64:291–5. doi:10.1136/ard.2004.022400. [PubMed: 15647438]

[79]. Eckstein F, Hudelmaier M, Putz R. The effects of exercise on human articular cartilage. J Anat 2006;208:491–512. doi:10.1111/j.1469-7580.2006.00546.x. [PubMed: 16637874]

[80]. Sutter EG, Liu B, Utturkar GM, Widmyer MR, Spritzer CE, Cutcliffe HC, et al. Effects of Anterior Cruciate Ligament Deficiency on Tibiofemoral Cartilage Thickness and Strains in Response to Hopping. Am J Sports Med 2019;47:96–103. doi:10.1177/0363546518802225. [PubMed: 30365903]

[81]. Taylor KA, Collins AT, Heckelman LN, Kim SY, Utturkar GM, Spritzer CE, et al. Activities of daily living influence tibial cartilage T1rho relaxation times. J Biomech 2019;82:228–33. doi:10.1016/j.jbiomech.2018.10.029. [PubMed: 30455059]

[82]. Schairer WW, Haughom BD, Morse LJ, Li X, Ma CB. Magnetic resonance imaging evaluation of knee kinematics after anterior cruciate ligament reconstruction with anteromedial and transtibial femoral tunnel drilling techniques. Arthrosc - J Arthrosc Relat Surg 2011;27:1663–70. doi:10.1016/j.arthro.2011.06.032.

[83]. Koff MF, Stanley DW, Weishaar PJ, Amrami KK, Kaufman KR. Short-term repeatability of joint space width measurements using a magnetic resonance imaging compatible knee positioning device. Proc Inst Mech Eng H 2010;224:1061–71. doi:10.1097/MPG.0b013e3181a15ae8.Screening. [PubMed: 21053771]

[84]. Martin KJ, Neu CP, Hull ML. An MRI-based method to align the compressive loading axis for human cadaveric knees. J Biomech Eng 2007;129:855–62. doi:10.1115/1.2800765. [PubMed: 18067389]

[85]. Stehling C, Baum T, Mueller-Hoecker C, Liebl H, Carballido-Gamio J, Joseph GB, et al. A novel fast knee cartilage segmentation technique for T 2 measurements at MR imaging - data from the Osteoarthritis Initiative. Osteoarthr Cartil 2011;19:984–9. doi:10.1016/j.joca.2011.04.002. [PubMed: 21515391]

[86]. Lüssea S, Claassen H, Gehrke T, Hassenpflug J, Schünke M, Heller M, et al. Evaluation of water content by spatially resolved transverse relaxation times of human articular cartilage. Magn Reson Imaging 2000;18:423–30. doi:10.1016/S0730-725X(99)00144-7. [PubMed: 10788720]

[87]. Koff MF, Shah P, Pownder S, Romero B, Williams R, Gilbert S, et al. Correlation of meniscal T2* with multiphoton microscopy, and change of articular cartilage T2 in an ovine model of meniscal repair. Osteoarthr Cartil 2013;21:1083–91. doi:10.1016/j.joca.2013.04.020. [PubMed: 23680878]

[88]. Gold GE, Thedens DR, Pauly JM, Fechner KP, Bergman G, Beaulieu CF, et al. MR imaging of articular cartilage of the knee: new methods using ultrashort TEs. Am J Roentgenol 1998;170:1223–6. doi:10.2214/ajr.170.5.9574589. [PubMed: 9574589]

[89]. Gatehouse PD, Bydder GM. Magnetic Resonance Imaging of Short T2 Components in Tissue. Clin Radiol 2003;58:1–19. doi:10.1053/crad.2003.1157. [PubMed: 12565203]

[90]. Robson MD, Gatehouse PD, Bydder M, Bydder GM. Magnetic Resonance: An Introduction to Ultrashort TE (UTE) Imaging. J Comput Assist Tomogr 2003;27:825–46. doi:10.1097/00004728-200311000-00001. [PubMed: 14600447]

[91]. Pauly JM, Conolly SM, Nishimura DG, Macovski A. A slice-selective excitation for very short T2 species. 7th Annu. Meet. SMR, 1989.

[92]. Du J, Bydder GM. Qualitative and quantitative ultrashort-TE MRI of cortical bone. NMR Biomed 2013;26:489–506. doi:10.1002/nbm.2906. [PubMed: 23280581]

[93]. Qian Y, Williams AA, Chu CR, Boada FE. Multicomponent T2* mapping of knee cartilage: Technical feasibility ex vivo. Magn Reson Med 2010;64:1427–32. doi:10.1002/mrm.22450.

[94]. Williams AA, Qian Y, Bear D, Chu CR. Assessing degeneration of human articular cartilage with ultra-short echo time (UTE) T2* mapping. Osteoarthr Cartil 2010;18:539–46. doi:10.1016/j.joca.2010.02.001. [PubMed: 20170769]

[95]. Williams AA, Qian Y, Chu CR. UTE-T2* mapping of human articular cartilage in vivo: A repeatability assessment. Osteoarthr Cartil 2011;19:84–8. doi:10.1016/j.joca.2010.10.018. [PubMed: 21035556]

[96]. Williams AA, Qian Y, Golla S, Chu CR. UTE-T2* mapping detects sub-clinical meniscus injury after anterior cruciate ligament tear. Osteoarthr Cartil 2012;20:486–94. doi:10.1016/j.joca.2012.01.009. [PubMed: 22306000]

[97]. Shao H, Chang EY, Pauli C, Zanganeh S, Bae WC, Chung CB, et al. UTE bi-component analysis of T2* relaxation in articular cartilage. Osteoarthr Cartil 2016;24:364–73. doi:10.1016/j.joca.2015.08.017. [PubMed: 26382110]

[98]. Goto H, Fujii M, Iwama Y, Aoyama N, Ohno Y, Sugimura K. Magnetic resonance imaging (MRI) of articular cartilage of the knee using ultrashort echo time (uTE) sequences with spiral acquisition. J Med Imaging Radiat Oncol 2012;56:318–23. doi:10.1111/j.1754-9485.2012.02388.x. [PubMed: 22697330]

[99]. Bae WC, Dwek JR, Znamirowski R, Statum SM, Hermida JC, D'Lima DD, et al. Ultrashort echo time MR imaging of osteochondral junction of the knee at 3 T: identification of anatomic structures contributing to signal intensity. Radiology 2010;254:837–45. doi:10.1148/radiol.09081743. [PubMed: 20177096]

[100]. Ma Y, Jerban S, Carl M, Wan L, Guo T, Jang H, et al. Imaging of the Region of the Osteochondral Junction (OCJ) Using a 3D Adiabatic Inversion Recovery Prepared Ultrashort Echo Time Cones (3D IR-UTE Cones) Sequence at 3T. NMR Biomed 2019;e4080. doi:10.1002/nbm.4080. [PubMed: 30794338]

[101]. Fullerton GD, Cameron IL, Ord VA. Orientation of tendons in the magnetic field and its effect on T2 relaxation times. Radiology 1985;155:433–5. doi:10.1148/radiology.155.2.3983395. [PubMed: 3983395]

[102]. Erickson SJ, Prost RW, Timins ME. The "magic angle" effect: background physics and clinical relevance. Radiology 1993;188:23–5. doi:10.1148/radiology.188.1.7685531. [PubMed: 7685531]

[103]. Rubenstein JD, Kim JK, Morova-Protzner I, Stanchev PL, Henkelman RM. Effects of collagen orientation on MR imaging characteristics of bovine articular cartilage. Radiology 1993;188:219–26. doi:10.1148/radiology.188.1.8511302. [PubMed: 8511302]

[104]. Henkelman RM, Stanisz GJ, Kim JK, Bronskill MJ. Anisotropy of NMR properties of tissues. Magn Reson Med 1994;32:592–601. doi:10.1002/mrm.1910320508. [PubMed: 7808260]

[105]. Mosher TJ, Smith H, Dardzinski BJ, Schmithorst VJ, Smith MB. MR Imaging and T2 Mapping of Femoral Cartilage. Am J Roentgenol 2001;177:665–9. doi:10.2214/ajr.177.3.1770665. [PubMed: 11517068]

[106]. Xia Y, Farquhar T, Burton-Wurster N, Lust G. Origin of cartilage laminae in MRI. J Magn Reson Imaging 1997;7:887–94. doi:10.1002/jmri.1880070518. [PubMed: 9307916]

[107]. Goodwin DW, Wadghiri YZ, Dunn JF. Micro-imaging of articular cartilage: T2, proton density, and the magic angle effect. Acad Radiol 1998;5:790–8. doi:10.1016/s1076-6332(98)80264-x. [PubMed: 9809078]

[108]. Mlynárik V, Szomolányi P, Toffanin R, Vittur F, Trattnig S. Transverse relaxation mechanisms in articular cartilage. J Magn Reson 2004;169:300–7. doi:10.1016/j.jmr.2004.05.003. [PubMed: 15261626]

[109]. Du J, Pak BC, Znamirowski R, Statum S, Takahashi A, Chung CB, et al. Magic angle effect in magnetic resonance imaging of the Achilles tendon and enthesis. Magn Reson Imaging 2009;27:557–64. doi:10.1016/j.mri.2008.09.003. [PubMed: 19022600]

[110]. Shao H, Pauli C, Li S, Ma Y, Tadros AS, Kavanaugh A, et al. Magic angle effect plays a major role in both T1rho and T2 relaxation in articular cartilage. Osteoarthr Cartil 2017;25:2022–30. doi:10.1016/j.joca.2017.01.013. [PubMed: 28161394]

[111]. Xia Y, Wang N, Lee J, Badar F. Strain-dependent T1 relaxation profiles in articular cartilage by MRI at microscopic resolutions. Magn Reson Med 2011;65:1733–7. doi:10.1002/mrm.22933. [PubMed: 21452280]

[112]. Wang N, Chopin E, Xia Y. The effects of mechanical loading and gadolinium concentration on the change of T1 and quantification of glycosaminoglycans in articular cartilage by microscopic MRI. Phys Med Biol 2013;58:4535–47. doi:10.1088/0031-9155/58/13/4535. [PubMed: 23760174]

[113]. Xia Y, Moody JB, Alhadlaq H. Orientational dependence of T2 relaxation in articular cartilage: A microscopic MRI (MicroMRI) study. Magn Reson Med 2002;48:460–9. doi:10.1002/mrm.10216. [PubMed: 12210910]

[114]. Xia Y, Zheng S, Bidthanapally A. Depth-dependent profiles of glycosaminoglycans in articular cartilage by MicroMRI and histochemistry. J Magn Reson Imaging 2008;28:151–7. doi:10.1002/jmri.21392. [PubMed: 18581328]

[115]. Kilian O, Wenisch S, Karnati S, Baumgart-Vogt E, Hild A, Fuhrmann R, et al. Observations on the microvasculature of bone defects filled with biodegradable nanoparticulate hydroxyapatite. Biomaterials 2008;29:3429–37. doi:10.1016/j.biomaterials.2008.05.003; 10.1016/j.biomaterials.2008.05.003. [PubMed: 18501961]

[116]. Zheng S, Xia Y. The collagen fibril structure in the superficial zone of articular cartilage by MicroMRI. Osteoarthr Cartil 2009;17:1519–28. doi:10.1016/j.joca.2009.05.013. [PubMed: 19527808]

[117]. Chen J, Carl M, Ma Y, Shao H, Lu X, Chen B, et al. Fast volumetric imaging of bound and pore water in cortical bone using three-dimensional ultrashort-TE (UTE) and inversion recovery UTE sequences. NMR Biomed 2016;29:1373–80. doi:10.1002/nbm.3579. [PubMed: 27496335]

[118]. Ma Y, Carl M, Shao H, Tadros AS, Chang EY, Du J. Three-dimensional ultrashort echo time cones T 1ρ (3D UTE-cones-T 1ρ) imaging. NMR Biomed 2017;30:e3709. doi:10.1002/nbm.3709.

[119]. Ma Y, Shao H, Du J, Chang EY. Ultrashort echo time magnetization transfer (UTE-MT) imaging and modeling: magic angle independent biomarkers of tissue properties. NMR Biomed 2016;29:1546–52. doi:10.1002/nbm.3609. [PubMed: 27599046]

[120]. Zhu Y, Cheng X, Ma Y, Wong JH, Xie Y, Du J, et al. Rotator cuff tendon assessment using magic-angle insensitive 3D ultrashort echo time cones magnetization transfer (UTE-Cones-MT) imaging and modeling with histological correlation. J Magn Reson Imaging 2018;48:160–8. doi:10.1002/jmri.25914. [PubMed: 29219218]

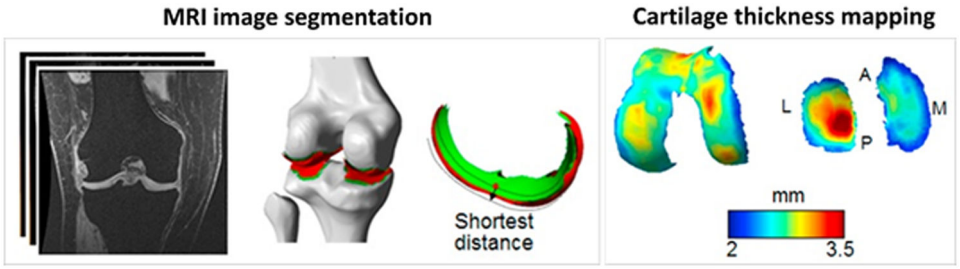

Figure 1:

Representative steps for thickness map measurement in tibiofemoral cartilage using MRI images and pixel-wise quantification. Wang et al. used MRI images from 3D-SPGR sequence with approximately 0.3×0.3×1.5 mm^3 voxel size to manually segment 3D geometries of bone and articular cartilage. Cartilage thickness was calculated as the shortest distance from the subchondral bone surface to articular surface in segmented cartilages. Contact region was defined as the overlapping areas of the femoral and tibial articular surfaces. A, P, M, and L refer to anterior, posterior, medial and lateral compartments of the cartilages, respectively. This figure is cropped from a figure presented previously by Wang et al. [26]; the reprinting permission is granted through Rightslink system.

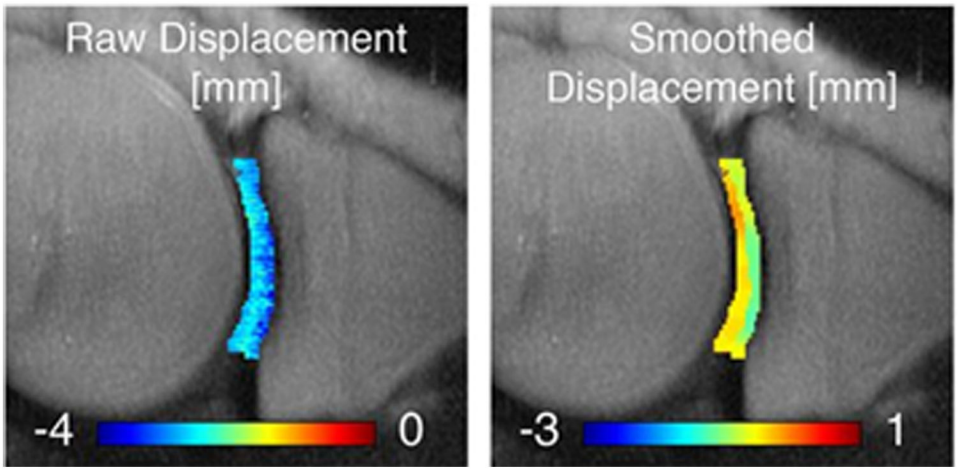

Figure 2:
Axial displacement map in sagittal slice of the tibiofemoral cartilage of medial knee joint under mechanical loading as measured with displacement encoding technique [31,36,37]. The figure is cropped from a previously presented figure by Chan et al. [31] based on Creative Commons permission guidelines (https://creativecommons.org/licenses/by/4.0/).

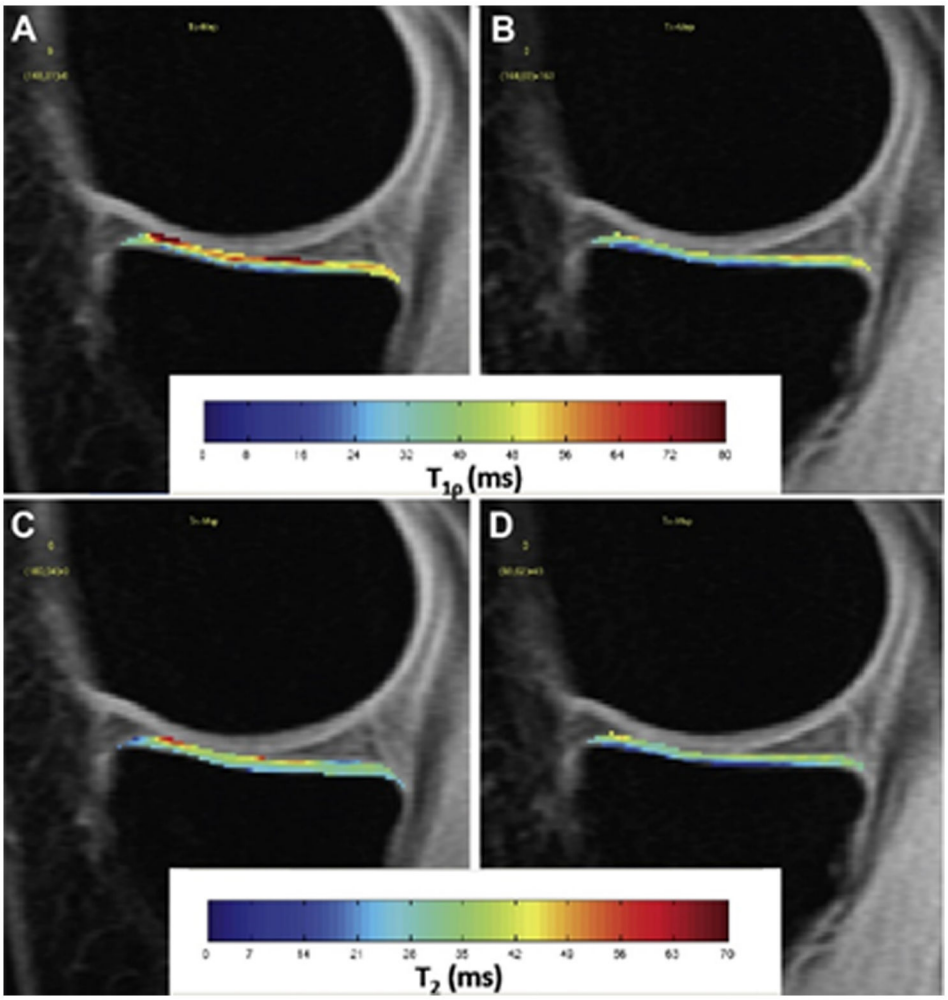

Figure 3:
Representative $T_{1\rho}$ (top row) and T2 (bottom row) maps of the medial tibial cartilage in the unloaded (A, C) and loaded (B, D) conditions. The figure is a figure previously presented by Souza et al. [47]. The reprinting permission is granted through Rightslink system.

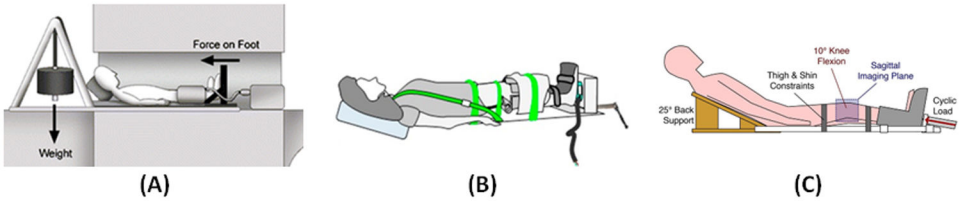

Figure 4:

(A) Schematic of a cable/pulley setup combined with a back-board and a sliding foot plate on low friction rollers to position the subject [34,44-50]. This schematic was previously presented by Cotofana et al. [44]. Reprinting permission is granted based on the open access license. (B) Schematic of the ratcheting mechanism driving an orthotic boot to apply mechanical load to the subject's feet, where an MRI-compatible load cell is attached for estimation of the applied load [26,27,83]. This schematic was previously presented by Wang et al. [26] and reprinting permission is granted through the Rightslink system. (C) Schematic of the active loading system utilizing an electro-pneumatic device [31]. The schematic was previously presented by Chan et al. [31] Reprinting is based on Creative Commons use guidelines (https://creativecommons.org/licenses/by/4.0/).

Table 1:

Summary of MRI-based loading studies performed on whole knee ex vivo or in vivo (studies are sorted based on the anatomical location and year of publication). PF and TF refer to patellofemoral and tibiofemoral cartilages.

Author/year	Anatomy /MRI output	Subjects/samples/ condition	Loading device	MRI sequence	Main findings
Herberhold, 1998 [29]	PF cartilage thickness	Human, 2 normal knees, ex vivo, 180% BW load	Pneumatic actuator	Fat-sat 3D GRE (FLASH), 1.5T, 0.3×0.3×2 mm^3	•10 and 30% thickness reductions in patellar cartilage for the first 10 min of loading
Herberhold, 1998 [28]	PF cartilage thickness/Fluid flux	Human, 6 normal knees, ex vivo, 150% BW	Pneumatic actuator	Fat-sat 3D GRE (FLASH), 1.5T, 0.3×0.3×2 mm^3	•Mean patellar cartilage deformation of 44% after 3.5 h •43% fluid loss in patellar cartilage after 3.5 h
Song 2006 [30]	TF cartilage thickness/ contact area/ strain	Sheep, 4 normal knees after meniscectomy, ex vivo, 150% BW	Pneumatic actuator	T1 weighted 3D GRE, 4.7T, 0.06×0.06×0.47 mm^3	•Significant decrease in the contact area and cartilage thickness
Nishii 2008 [23]	TF cartilage T2	Human, 22 normal knees, in vivo, 50% BW	Suspended weights/ rope & pulley system	T2-weighted spin echo, 3T, 0.2×0.2×3 mm^3	•T2 decreased under loading over the tibial cartilage, but only in the contact region with the femoral cartilage
Chan 2009 [36,37]	TF cartilage deformation and strain	Porcine, 8 normal knees, ex vivo, 200% BW	Pneumatic actuator	DENSE-FSE, 7T, 0.3×0.3×2 mm^3	•Deformation and strains were heterogeneous through the depth of TF cartilage •Loading direction strains were maximal in the middle zone of TF cartilage
Shiomi 2010 [24]	TF cartilage T2	Porcine, 10 normal knees, ex vivo, 33% BW	Compressed elastic elements	T2-weigted spin echo and SPGR, 3T, 0.3×0.4×3 mm^3	•Greatest decrease of T2 was in intermediate zone of the cartilage. •The T2 reduction correlated with contact pressure measured with sensitive films placed in the knee joints
Souza 2010 [34]	TF cartilage T2 and T1ρ	Human, 10 normal and 20 OA knees, in vivo, 50% BW	Suspended weights/ rope & pulley system	T1ρ- and T2-weighted 3T, 0.4×0.7×2 mm^3	•Significant reductions of T2 and T1ρ under mechanical loading were found only at the medial joint.
Mayerhoefer 2010 [22]	TF cartilage T1-Gd	Human, 22 normal knees, in vivo, 50% BW	Pneumatic actuator	GRE T1-GD , 3T, 0.4×0.4×3 mm^3	•Significant decrease in average T1-Gd was observed for joints under loading
Cotofana 2011 [44]	TF cartilage thickness/ contact area	Human, 11 normal and 19 OA knees, in vivo, 50% BW	Suspended weights/ rope & pulley system	Fat-sat GRE (SPGR) 3T, 0.4×0.8×1.5 mm^3	•Significant reduction in cartilage thickness for medial tibia and femoral contact points
Shin 2011 [42]	TF cartilage contact area	Human, 10 normal and 11 OA knees, in vivo, 50% BW	Suspended weights/ rope & pulley system	Fat-sat GRE (SPGR) 0.3×0.3×1.5 mm^3 and T2-weighted FSE, 0.3×0.4×2 mm^3, 3T	•TF contact areas in significantly increased by loading with greater increases in medial joint •For both unloaded and loaded conditions medial joint showed larger contact areas in OA joints
Butz 2011 [38]	TF cartilage deformation, strain/stress	Porcine, 7 normal knees, ex vivo, 100% BW	Pneumatic actuator	DENSE-FSE, 7T, 0.3×0.3×2 mm^3	•A nonlinear FEA model was appropriate to predict the characterization of stresses in cartilage
Subburaj 2012 [46]	TF cartilage thickness/ contact area / T1ρ and T2	Human, 10 healthy and 20 OA knees, in vivo, 50% BW	Suspended weights/ rope & pulley system	SPGR and FSE, 0.3×0.3×2 mm^3, plus T1ρ- and T2- weighted, 0.3×0.5×3 mm^3, 3T	•Greater cartilage thickness changes in medial joint

Author/year	Anatomy /MRI output	Subjects/samples/ condition	Loading device	MRI sequence	Main findings
					•Superficial layers showed higher changes in T1ρ and T2 vs. whole cartilage •The average changes of T1ρ, T2, and cartilage thickness were higher in OA vs. normal subjects.
Shiomi 2012 [68]	TF cartilage T2	Porcine, 10 normal knees undergo meniscectomy, ex vivo, 33% BW	Compressed elastic elements	T2-weighted spin echo, 3T, 0.3×0.4×3 mm^3	•Regions with T2 decreases of medial joint under loading shifted from anterior/central to posterior sites after meniscectomy
Souza 2014 [47]	TF cartilage T2 and T1ρ	Human, 93 normal and 44 OA knees, in vivo, 50% BW	Suspended weights/ rope & pulley system	FSE CUBE, 0.4×0.4×0.5 mm^3, T1ρ- and T2-weighted, 0.5×1×4 mm^3, 3T	•Significant decreases of T1ρ and T2 were found at the superficial layer yet significant increases at deep layer for both groups •Reductions were grater for subjects with OA
Wang 2015 [26]	TF cartilage thickness, strain map	Human, 4 normal knees, in vivo, 50% BW	Ratcheting mechanism plus a load cell	SPGR, 3T, 0.3×0.3×1.5 mm^3	•Significant strain increases were found in medial femoral, lateral femoral and lateral tibial cartilages
Chan 2016 [31]	TF cartilage deformation, strain and stress	Human, 9 normal knees, in vivo, 50% BW	Pneumatic actuator	DENSE-FSE, 3T, 0.3-0.7×0.3-0.7×3 mm^3	•Correlations between body mass index and maximum principle and shear strain measures in tibial cartilage were reported
Maher 2017 [27]	TF cartilage thickness, strain map	Human, 5 knees undergoing meniscectomy, in vivo, 50% BW	Ratcheting mechanism plus a load cell	SPGR, 3T, 0.3×0.3×1.5 mm^3	•The MR-based cartilage deformation pattern was consistent with contact stress map measured directly by sensors
Szomolanyi 2017 [41]	TF cartilage T2	Human, 10 normal knees, in vivo, 250 N	Pneumatic actuator	TESS, 0.3×0.3×1.5 $mm^3$7T	•T2 reduction was found for regions under loading while T2 increase was observed for regions adjacent to load bearing cartilage.
Zevenbergen 2018 [39]	TF cartilage deformation, strain and stress	Bovine, 8 normal and 8 defected knees, ex vivo, 50% BW	Pneumatic actuator	DENSE-FSE, 9.4T, 0.1×0.1×1 mm^3	•Elevated strains at the defect regions of the cartilage were reported. •Minimal increase in strain patterns in the opposing cartilage was found at contact with the defect region.
Stehling 2012 [43]	Meniscus extrusion plus morphology of meniscus and cartilage	Human, 10 normal and 20 OA knees, in vivo, 50% BW	Suspended weights/ rope & pulley system	SPGR, 0.3×0.3×1.5 mm^3 and fat-sat T2-weighted FSE, 0.4×0.7×2 mm^3 , 3T	•Significantly greater increase in meniscus extrusion was reported for degenerated knees under loading compared with normal knees. •In knees with higher OA scores, loading resulted in larger morphological changes in meniscus and cartilage
Subburaj 2015 [48]	Meniscal T2 and T1ρ	Human, 10 normal and 20 OA knees, in vivo, 50% BW	Suspended weights/ rope & pulley system	SPGR and FSE, 0.3×0.3×2 mm^3, plus T1ρ- and T2-weighted, 0.3×0.5×3 mm^3, 3T	•T2 and T1ρ increases were reported in meniscus under loading •Significantly higher variations were reported for controls compared with OA subjects
Patel 2016 [50]	Meniscus extrusion	Human, 56 normal and 78 OA knees, in vivo, 50% BW	Suspended weights/ rope & pulley system	FSE CUBE, 0.4×0.4×0.5 mm^3, T1ρ-	•Significant differences in medial meniscal extrusion between loading and

Author/year	Anatomy /MRI output	Subjects/samples/ condition	Loading device	MRI sequence	Main findings
				and T2-weighted, 0.5×1×4 mm^3, 3T	unloading for the entire cohort. •Healthier knees showed lower meniscal extrusion variation under loading
Calixto 2016 [49]	Meniscal T2 and T1ρ	Human, 85 normal and 39 OA knees, in vivo, 50% BW	Suspended weights/ rope & pulley system	FSE CUBE, 0.4×0.4×0.5 mm^3, T1ρ- and T2-weighted, 0.5×1×4 mm^3, 3T	•A significant increase with loading was seen in the T2 of the control group, while T2 increase was less frequently observed in subjects with OA.
Hornakova 2018 [40]	Meniscal T2*	Human, 4 normal knees, in vivo, 50% BW	Tightened rubber bands plus dynamometric insoles	GRE, 3T, 0.7×0.7×1.3 mm^3	•A constant significant increase of T2* under loading was reported in the anterior horn of the medial meniscus